AIAA 82-4309

Attitude Control of a Satellite with a Rotating Solar Array

J.P. Chrétien,* C. Reboulet,* and P. Rodrigo*
Centre d'Etudes et de Recherches de Toulouse (CERT/DERA), Toulouse, France
and
M. Maurette*
Centre National d'Etudes Spatiales, Toulouse, France

This paper describes the dynamic modeling and fine pointing control system design for the SPOT French Earth observation satellites. The dynamic model of the vehicle includes a representation of the flexible solar array by effective mass technique. An onboard computer processes the attitude rate information provided by a gyro package and, possibly, the measurement of torque around boom axis to provide a very high angular rate accuracy with the help of reaction wheels and solar array drive motor. Several control design techniques are investigated for this multivariable control problem. Performances, including sensitivity to modal data, are checked by extensive simulations.

I. Introduction

EARTH observation satellites differ mainly from other satellites (scientific, telecommunications, television) in the strong requirements on attitude rates of the spacecraft during the operational observation mode. A great deal of the control design is then directed by the short term torque disturbances; the dynamic reactions of the payload itself and of the flexible solar array give major contributions. Moreover, this array is mounted dissymmetrically on the spacecraft in order to avoid payload interaction.

The control of a satellite with flexible appendages often has been investigated, the concern centering on the stability of the closed-loop control laws; in the Earth observation case, a problem of performance appears, particularly when harmonic disturbances are considered. The solar pointing mechanism of the power generator induces such disturbances and the present paper is devoted to a detailed investigation of these problems and their solutions in the frame of the SPOT French Earth observation project.[1]

II. Satellite Organization and Mission

SPOT is a French Earth observation program using the same multimission platform (PFM) for several payloads. This PFM platform provides attitude and orbit control for the Earth-pointing satellites operating on circular heliosynchronous orbits.[2] The system is designed to operate in the 600-1200-km altitude range and provides a highly accurate pointing stability (typically, $3\ 10^{-4}$ deg/s each axis) with moderate absolute pointing accuracy (0.05 deg). The PFM also provides the power supply through a folded, large flexible solar array (about 24 m^2) oriented toward the sun by a single degree of freedom articulation called Mécanisme d'Entrainement du Générateur solaire (MEGS). This articulation includes power slip-rings giving a perturbating friction torque, and a driving motor. It can be fitted with a torquemeter around the broom axis. The first satellite of this family will be put in a 800-km orbit with a payload including a high resolution telescope with push-broom scanning technique and a tape recorder that is used for data storage and gives an exponentially shaped disturbance torque when started or stopped (peak value, 0.25 Nm).

Received Sept. 30, 1981; revision received May 25, 1982.

*Research Engineer.

The side-view mirror of the satellite is actuated by a stepping motor (8-Hz frequency) inducing a torque, the model of which is the superposition of a sinusoid and two opposite impulses.

A general view of the satellite described herein is shown in Fig. 1. The studies presented in this paper are related only to the high-accuracy operating mode and, therefore, only the specific elements of this mode will be described.

Sensors

A rate gyro package gives the attitude rate of the satellite while a double scanning Earth sensor gives the pitch and roll information. Best estimates of the attitude and of the gyro drifts are given by a Kalman filter. Since yaw gyro drift is unobservable with these sensors, yaw information is collected once an orbit by an additional sun sensor. The Kalman filter is operated at a very low frequency so that it can be neglected for stability studies.

Gyro bandwidth is 5 Hz and output noise $1.2\ 10^{-6}$ s. To improve performance and stability margins an extra (optional) sensor may be available; a piezoelectric torquemeter measures the reaction torque of the solar array on the satellite body through a high-pass filter (cutoff frequency, 0.05 Hz) with a $0.7\ 10^{-4}$ Nm output noise up to 10 Hz.

Actuators

Torque actuation is completed by three reaction wheels with a maximum available torque of 0.1 Nm and two magnet coils to avoid saturation. The MEGS motor can be used as a second pitch actuator. This motor being driven like a synchronous motor following the orbital speed, a torque between the vehicle's body and the solar array can be obtained by varying the synchronous speed and/or giving it a phase shift. The maximum variation of the synchronous speed must not exceed the orbital angular velocity. Since the motor has 300 poles, the nominal driving period will be 20 s (orbital period $\simeq$90 min) so that the defects of the teeth will induce periodical perturbations at the following frequencies: 0.05, 0.1, 0.2, and 0.4 Hz. The fourth harmonic (0.2 Hz) gives the higher torque: 0.05 Nm.

Onboard Computer

All the information is digitized and fed hrough a sampled data bus to a central computer performing the filtering and the control laws.

Sample data frequency is $T=8$ Hz and maximum delay in the control loop will be 60 ms (typically, 30 ms).

III. Dynamic Modelling of the Spacecraft

Dynamic Representation of the Solar Array

Effective Mass Concept

The effective mass concept[3] is used to describe the dynamic behavior of the array structure: a generalized relationship between forces and torques F_p and C at the link point P between array and vehicle and linear and angular accelerations γ_p and $\dot{\omega}$ of that same point (Fig. 2)

$$\begin{bmatrix} F_p \\ C \end{bmatrix} = M(s) \begin{bmatrix} \gamma_p \\ \dot{\omega} \end{bmatrix} \tag{1}$$

The 6×6 dynamic matrix $M(s)$ may be decomposed over the modal basis under two forms

$$M(s) = M_r + \sum_{k=1}^{N} M_k T_k(s) = M_0 - \sum_{k=1}^{N} M_k' H_k(s) \tag{2}$$

The second one introduces the "static mass" M_0, a generalized mass matrix representing the structure supposed rigid at point P; while the first one introduces the "residual mass" M_r, representing the part of the structure which is not taken into account by the N modes considered. M_k and M_k' are 6×6 constant matrices and $T_k(s)$ and $H_k(s)$ are transfer functions which may be written, respectively (with the conservative hypothesis),

$$H_k(s) = \frac{\omega_k^2}{s^2+\omega_k^2} \qquad T_k(s) = \frac{s^2}{s^2+\omega_k^2} \tag{3}$$

The dynamic description of the structure is then defined by the following data: N values of the modal frequencies ω_k, N 6×6 matrices M_k and either matrix M_0 or matrix M_r.

State Space Representation of the Structure

Further, matrices M_k may be written

$$M_k = L_k L_k^T \tag{4}$$

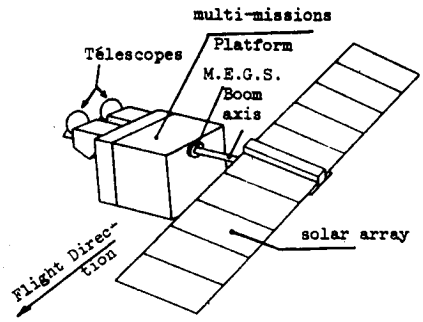

Fig. 1 Schematic view of the satellite.

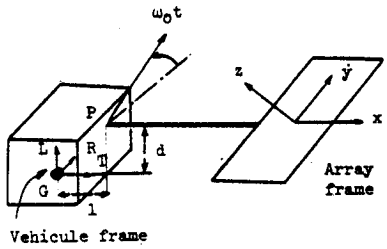

Fig. 2 Vehicle and array schematic.

where L_k is a 6×1 column vector. Then, only six values are needed to define each matrix.

This property is important when a state space representation is desired. The whole representation

$$\dot{X} = AX + B\gamma \qquad \gamma = \begin{bmatrix} \gamma_p \\ \dot{\omega} \end{bmatrix} \qquad F = \begin{bmatrix} F_p \\ C \end{bmatrix} \tag{5a}$$
$$F = CX + D\gamma$$

is obtained as the direct sum of two-dimensional subspaces which equations read

$$\dot{X}_i = \begin{bmatrix} 0 & -1 \\ \omega_i^2 & 0 \end{bmatrix} X_i + \begin{bmatrix} L_i^T \\ 0 \end{bmatrix} \gamma \tag{5b}$$

$$F_i = \begin{bmatrix} 0 & L_i \end{bmatrix} X_i$$

and direct transmission matrix D is equal to matrix M_r.

Derivation of the Whole Dynamic Model

The whole dynamic model will be obtained by equating the accelerations γ' of point P, considered as belonging to the vehicle, as equal to the accelerations γ of point P belonging to the array, while forces F' are opposite to forces F. The dynamic relationship between forces F' and accelerations γ' at point P of the rigid vehicle must then be derived. Introducing external forces F_l and external torques C_l on the vehicle of mass m_v and center of mass G, one may write

$$\gamma_p' = \frac{F_p' + f_l}{m_v} + \dot{\omega}' \Lambda GP; \qquad F' = \begin{bmatrix} F_p' \\ C' \end{bmatrix} \quad \gamma' = \begin{bmatrix} \gamma_p' \\ \dot{\omega}' \end{bmatrix}$$

$$\Pi_G \dot{\omega}' = C_l + C' + GP\Lambda F_p' \quad F_l = \begin{bmatrix} f_l \\ C_l \end{bmatrix} \tag{6}$$

where the quadratic terms in ω, e.g., $\omega\lambda(\Pi\omega)$, have been neglected due to the small angular rates which will be considered, and where the external forces are applied to the center of mass of the vehicle.

These relations may be summarized in matrix form, introducing the antisymmetric tensor $^*GP$ associated with vector GP.

$$\begin{bmatrix} F_p' \\ C' \end{bmatrix} = \left[\begin{array}{c|c} m_v I & m_v(^*GP) \\ \hline -m_v(^*GP) & \Pi_G - m_v(^*GP)^2 \end{array}\right] \begin{bmatrix} \gamma_p' \\ \dot{\omega}' \end{bmatrix} + \begin{bmatrix} -I & 0 \\ ^*GP & -I \end{bmatrix} \begin{bmatrix} f_l \\ C_l \end{bmatrix} \tag{7a}$$

that is,

$$F' = M_v \gamma' + N_v F_l \tag{7b}$$

The dynamic model of the whole spacecraft is then readily obtained using Eqs. (5a) and (7a), and the state-space equations read

$$\dot{X} = [A - B(M_v + D)^{-1} C]X + B[(M_v + D)^{-1} D - I] M_v^{-1} N_v F_l$$
$$\gamma' = -(M_v + D)^{-1} Cx + [(M_v + D)^{-1} D - I] M_v^{-1} N_v F_l \tag{8}$$

The angular stabilization problem mainly is concerned with the relationships between the last three components of F_l and the last three components of γ'.

The coupling of the equations is more complicated when a magnetic stiffness K_m is introduced in the array drive motor, along the pitch axis. A torque f_4 proportional to the angular gap between stator and rotor must be introduced

$$f_4 = K_m(\theta_s - \theta_r) \tag{9}$$

where θ_s and θ_r are, respectively, the inertial attitude of the stator (i.e., the vehicle) and the rotor (i.e., the array). The further derivations of the dynamic equations are different depending on element d_{44} of matrix M_r. A supplementary mode, corresponding to the resonator obtained with K_m and the ensemble movement of the array around the pitch axis, appears if this inertia is not zero; its frequency decreases with increasing residual inertia.

Introduction of SPOT Data

The preceding considerations are illustrated by data for the SPOT array (four most significant modes); the axes in which these data are given are the array geometrical frame (Fig. 2); namely, x along the boom, y along the wing, and z normal.

$\omega_1 = 0125$ Hz $\quad L_1 = [0,\ 0,\ 0,\ 23.2,\ 0,\ -7.3]$

$\omega_2 = 0.206$ Hz $\quad L_2 = [2.5,\ 0,\ 9.5,\ 0,\ 23.4,\ 0]$

$\omega_3 = 0.124$ Hz $\quad L_3 = [0,\ -5.7,\ 0,\ 5.8,\ 0,\ 33.2]$

$\omega_4 = 0.644$ Hz $\quad L_4 = [0,\ 9.6,\ 0,\ 2.3,\ 0,\ -9.4]$

A residual inertia of 24 m^2 kg remains on the pitch axis, to be compared to a total static inertia of 600 m^2 kg.

Derivation of a Simplified Model

The quasiallocation of each mode to each rotational axis leads to the idea of a simplification of the modal data in order to obtain a transfer function simplified model. The three first modes are considered and in each of them the major translational and rotational component only is retained, leading to the modal vectors

$$L_1' = [0,\ 0,\ 0,\ 23.2,\ 0,\ 0]$$

$$L_2' = [0,\ 0,\ 9.5,\ 0,\ 23.4,\ 0]$$

$$L_3' = [0,\ -5.7,\ 0,\ 0,\ 0,\ 33.2]$$

In addition, the vehicle is supposed to have equal inertias on roll and yaw axes; and the distance between the centers of mass of the vehicle alone and with the array is negligible.

The description of the spacecraft is completed by abscissa 1 of point P in the vehicle frame, by distance d between vehicle pitch axis and array boom, and by value of the orbital frequency ω_0 which allows the calculation of the angle of rotation of the array with respect to the vehicle ($\omega_0 t$).

It is then possible to solve Eq. (7a) in the array frame and to get a transfer function block diagram of the dynamical relationships between the control torques and the vehicle angular rates resolved in this frame (Fig. 3).

F_i and H_i are second-order transfer functions which read, respectively,

$$F_i = \frac{s^2 + \omega_i^2}{s^2 + \Omega_i^2} \qquad H_i = \frac{\omega_i^2}{s^2 + \omega_i^2}$$

ω_i's are the modal frequencies and Ω_i's are obtained from modal and dynamical data. A very interesting feature is that coefficients A, B, C', and C'' are proportional to distance d. The coupling between the three open-loop transfer functions describing respectively the dynamics on the pitch axis, along the array wing, and normal to it is zero if the boom axis goes through the vehicle center of mass. The splitting of the three axis problem into three single axis problems is then less and less valid as distance d grows.

Evolution of the Dynamical Model along the Orbit

An illustration of this validity may be found using the precise complete model established in the preceding section. The transfer matrix between external vehicle torques (e.g., control torques) and angular accelerations resolved either in the vehicle frame or in the array frame may be calculated easily from the state-space representation and attention is focused on its diagonal elements. The variations of their poles and zeros have been drawn as a function of the angle of rotation of the array with respect to the vehicle as the orbit is described (Figs. 4a and 4b). An approximation of these transfer functions to one mode each is checked for validity in the array frame, in which the mode frequencies are shown much more stationary than in the vehicle frame. It then seems sound first, to decouple the pitch control problem from the "roll-yaw" control problem; and second, to decouple the roll from the yaw by controlling the angular rate resolved in the array frame. This introduces the control problem and its solutions, which will be investigated in the next section.

IV. Control Laws Design

Roll-Yaw Control Design

Control Law Structure

As indicated in the previous section, the simplified model derivation leads to the idea of a regulation of the attitude rate in the array frame (i.e., in the inertial frame), in which the modal characterization of each open-loop transfer function remains almost stationary along the orbit. The attitude itself is regulated in the spacecraft frame. Figure 5 shows the two imbedded loops, the inner one with the resolution of the gyro measurements in the array frame, the outer one elaborating the setpoint in attitude rate. This requires knowledge of the anomaly of the orbit, which already exists in the onboard computer.

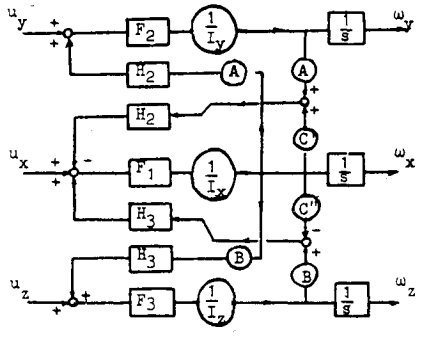

Fig. 3 Simplified model block diagram.

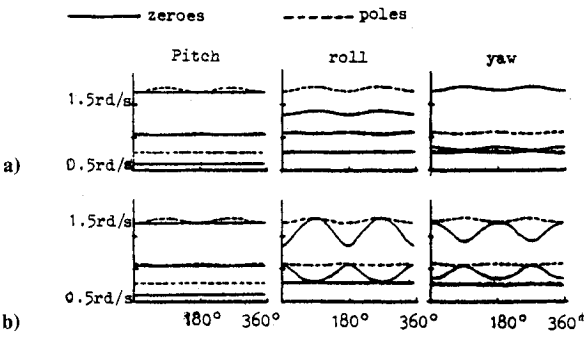

Fig. 4 Poles and zeros of major transfer functions (three modes simplified model) in array and vehicle axes; a) array axes and b) vehicle axes.

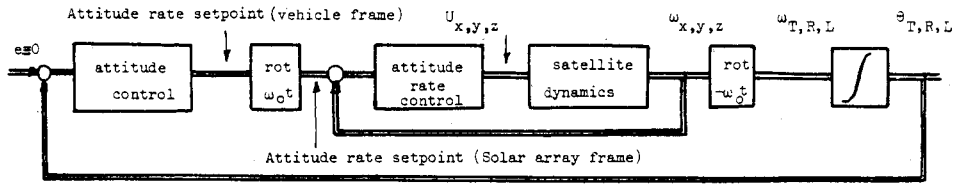

Fig. 5 Roll yaw control structure.

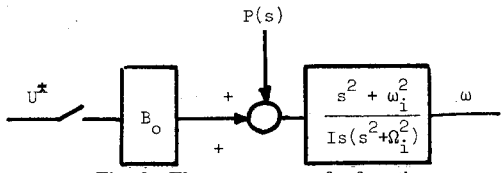

Fig. 6 Elementary transfer function.

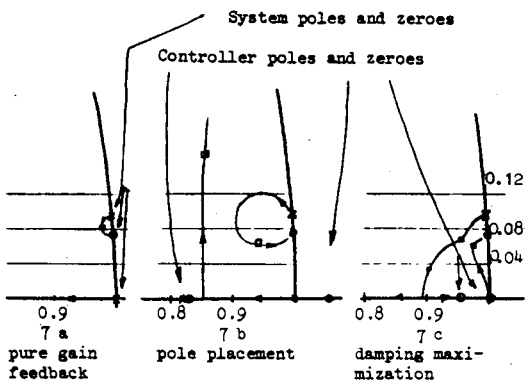

Fig. 7 Root loci for various control laws (elementary problem).

Control Law Synthesis for the Elementary Transfer Function

The inner transfer function then takes the form shown in Fig. 6 on each axis ($i=1,2$, or 3), where the control variable u is used to regulate the vehicle attitude rate ω in spite of disturbances $P(s)$.

The relationship between the sampled signal ω^* and the sampled and held control u^* reads approximately (up to the third order in $\Omega_i T$)

$$\frac{\omega^*}{u^*} = \frac{T}{I}\left[1-\frac{(\Omega_i^2-\omega_i^2)T^2}{6}\right]\frac{Z^{-1}}{1-Z^{-1}}\,\frac{1-2\cos\omega_i TZ^{-1}+Z^{-2}}{1-2\cos\Omega_i TZ^{-1}+Z^{-2}} \tag{10}$$

From the pole-zero configuration point of view, the continuous imaginary roots are then transformed into roots on the unit circle; if the product $\Omega_i T$ is sufficiently small, the neighborhood of the origin in s is transformed into the neighborhood of point (1,0) in the Z plane.

Three syntheses of a control law insuring a sufficient damping in closed loop (which is the major requirement due to the mirror disturbance) may be considered.

The first, feedback of a pure gain, allows choice of either the low-frequency mode or the "flexible" mode closed-loop damping (Fig. 7a), but not both; the maximum damping of the flexible mode may not be sufficient, as we will see later in the pitch case, but the closed loop is robust with respect to the frequency variations.

The second, pole placement, is a second-order controller which allows arbitrary location of all five closed-loop roots. For instance, the flexible mode may be damped down to 0.7, the other closed-loop roots being chosen faster and also well damped. The resulting controller (Fig. 7b) shows a zero slightly off the unit circle near point 1, a dipole in the medium frequency band, and a "fast" pole. The freedom in the closed-loop location, however, is paid for from three points of view: the static gain of the controller (and precision problems could occur for too great constant disturbing toques); the noise transmission of the loop; and the sensitivity to frequency variations.

The third synthesis is intermediate solution. A first-order controller may be considered to get a good compromise between the number of controller parameters used to tune the control law and the robustness of the control; the following control law is introduced:

$$D(Z) = \frac{U(Z)}{\epsilon(Z)} = K\frac{1-AZ^{-1}}{1-Z^{-1}} \tag{11}$$

relating the rate error ϵ to the control torque u. A supplementary pole at point 1 and a 0 at point A are then considered and root locus techniques lead to determination of K and A (Fig. 7c). It is worth noting that a systematic way to maximize the global closed-loop damping may be derived in the continuous case. Let the transfer function

$$\frac{1}{s}\,\frac{s^2+\omega_i^2}{s^2+\Omega_i^2}$$

be controlled through controller $k_1/s+k_2$. The characteristic equation reads

$$s^4+k_2s^3+(\Omega_i^2+k_1)s^2+k_2\omega_i^2s+k_1\omega_i^2=0 \tag{12a}$$

It may be split into a product of two trinoms

$$(s^2+2\delta s+\omega_1^2)(s^2+2\delta s+\omega_2^2) \tag{12b}$$

where δ is the common maximum absolute damping desired ($\xi_1\omega_1=\xi_2\omega_2=\delta$). Derivation of the calculation leads to

$$\omega_1^2=\omega_2^2=\omega_i^2 \qquad \delta^2=(\Omega_i^2-\omega_i^2)/4 \tag{13}$$

The two pairs of complex and conjugate roots are then identical. Application of this to the roll-yaw control loop shows that a relative damping of 0.4 for each loop can be obtained. It depends only on the classical "inertia ratio" $\sqrt{1-(\omega_i^2/\Omega_i^2)}$ of the loop considered, which happens to be almost the same on the three axes for the SPOT data.

The level of performances is much less affected than in the preceding case (pole placement) to the mode frequency variations, however, it may be shown that it is better to design the controller coefficients for minimum rather than for nominal value. The digital controller then is obtained by bilinear transformation which is quite valid due to the great sampling frequency with respect to the mode.

The global control loop is built by elaborating the attitude rate setpoint from the attitude discrepancy. This external loop, which is not affected by disturbing torques, is made much slower than the inner one to avoid dynamic coupling between them. A simulation built from the simplified model block diagram insured that each elementary loop works satisfactorily and that the couplings did not introduce stability problems at their simplified level.

Pitch Axis Control Law Design

Reaction Wheel Control

The pitch control loop may be first considered in the same manner as the roll and yaw loops, ignoring the possibilities of actuation by the array drive motor (MEGS). A similar first-order control network may be selected. However it is not satisfactory for two reasons:

1) The attitude rate does not meet the specifications in the desired response time for the tape recorder (10 s after start/stop).

2) The harmonic closed loop gain at the fourth harmonic (0.2 Hz) of the MEGS disturbance is much over the requirements.

The second drawback is more boring than the first ones as it affects the pointing performances during the whole fine pointing mode. The following sections are then dedicated to the two-input problem with the reaction wheel and the MEGS.

Introduction of the Array Drive Motor Control

Basic open loop scheme

The introduction of the MEGS control modifies Eq. (9) in the following manner.

$$f_4 = K_m(\theta_s - \theta_r + \theta_c) + \Gamma = K_m \int (\omega_s - \omega_r + \omega_c)\,dt + \Gamma \quad (14)$$

where θ_c is the desired relative angle between rotor and stator of the drive and Γ the disturbing torques of the motor. It then is possible to represent the open loop in the manner indicated in Fig. 8. The two actuators appear clearly as well as the two sources of disturbance Γ and C_u (the payload disturbances and the couplings from the other axis).

The transfer function $G(s)$ (equal to $[\omega_f^2 - \Omega_f^2)/(s^2 + \Omega_f^2)]$ in the case of one mode) is replaced by a higher-order transfer function when other modes are introduced on the pitch axis. It, however, may be written

$$G(s) = -\sum_{i=1}^{N} \frac{K_i}{s^2 + \Omega_i^2} \quad (15)$$

Control law analysis in low frequency

The control law analyzed is obtained by a simple gain on each of the individual feedbacks from the gyro measurement toward the reaction wheel and the MEGS

$$u_x^* = a(\omega_{x_c}^* - \omega_x^*) \qquad \omega_c^* = c\omega_x^* \quad (16)$$

where ω_{x_c} is the setpoint delivered by the outer loop.

The second loop is first closed for the needs of the analysis. It then may be shown that an approximation of the discretized transfer function reads (subscript t for pitch axis)

$$\frac{\omega_x^*}{\omega_c^*} \simeq \frac{(\omega_t^2 - \Omega_t^2)T^2}{2} \frac{Z^{-1}(1 + Z^{-1})}{1 - 2\cos\Omega_t T Z^{-1}} \quad (17)$$

Using approximation Eq. (10) of the further open-loop transfer function between reaction wheel and gyro

$$H(Z) = \frac{\omega_x^*}{U_x^*} \simeq \frac{T}{I_x}\left[\frac{1 - (\Omega_t^2 - \omega_t^2)T^2}{6}\left(\frac{Z^{-1}}{1 - Z^{-1}}\right)\right] \times \frac{(1 - 2\cos\omega_t T Z^{-1} + Z^{-2})}{(1 - \alpha Z^{-1})(1 - \bar{\alpha} Z^{-1})} \quad (18)$$

where α and $\bar{\alpha}$ are given by root locus of

$$1 + cZ[B_0 G(s)] = 0 \quad (19)$$

after Z transformation of the transfer function $B_0 G(s)$. These roots are on a circle centered at point $(-1,0)$ and passing through the images of the open-loop pole $e^{\pm j\Omega_t T}$. Then, as c is varied, the root locus corresponding to variations of a starts from a pole which moves on this circle, to arrive at zero remaining at the same position (transform of the open loop zero by $e^{\pm j\omega_c E}$).

Let us now (Fig. 9) represent the vicinity of point $(+1,0)$ in the Z plane where circles centered at the origin and at point $(-1,0)$ have been confused; a set of root loci (lead parameter a) may be drawn for varying c and a few of them have been indicated. It is clear that for increasing c, the maximum damping achievable is more and more important. An approximate evaluation of the amplitude for a harmonic disturbing torque may even be derived, and a trimming of the control law, just sufficient to insure the performances for harmonic inputs, may be established.

This may be interpreted as an increase of the distance between the open-loop pole and the open-loop zero (by means of the gyro to MEGS feedback) to get a better closed-loop damping. Another possibility shown on the figure is to let the open-loop pole cancel the open-loop zero by making $c = -1$; that is, $\omega_c^* = \omega_x^*$. This corresponds clearly to having the rotor fixed in the inertial frame; no vehicle disturbance will be transmitted to the array. This could help for the start/stop tape recorder problem (as a temporary control mode) but is of no use as far as harmonic components are considered.

Influence of the higher-order modes

This introduction of the array drive control leads to satisfactory results for the significant pitch flexible mode. The

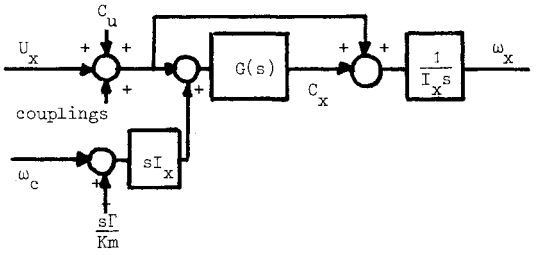

Fig. 8 Pitch axis block diagram.

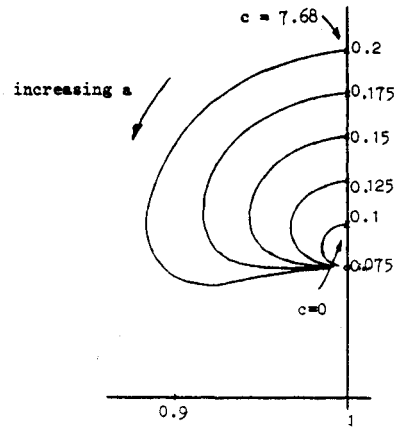

Fig. 9 Set of root loci for the pitch control problem.

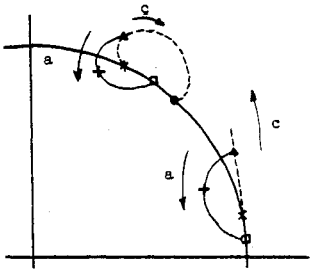

Fig. 10 Pitch axis root locus (two modes in Z plane).

analysis, however, may be generalized for a transfer function $G(s)$, as expressed in Eq. (15), under the hypothesis $\max \Omega_l T < \pi$. The transfer function between u^* and ω_x^* reads

$$\frac{\omega^*}{u^*} = \frac{Z\left[B_0\left(\frac{1+G}{I_x s}\right)\right]}{1 - cZ[B_0 G]} \tag{20}$$

and a detailed analysis shows the following.

1) The zeros of the denominator transfer function lie on the root locus (lead variable $-c$) associated to transfer function $Z[B_0G]$; which is itself split into alternating poles and zeros around the unit circle (crosses and arcs of Fig. 10). This property leads to instability of the array drive feedback alone for all pitch flexible modes considered. The effective poles are located on the triangles.

2) The zeros of the numerator transfer function lie on the unit circle between the preceding poles and zeros (squares of Fig. 10).

3) The numerator and denominator transfer functions have the same poles.

Then, the root locus describing the characteristic equation of the closed-loop system has arrival points on the squares, and starting points on the triangles, obtained for a certain value of c.

Figure 10 then shows clearly that the destabilizing effect is more and more important as the mode frequency increases. It is worth noting that this does not happen in the continuous case, where all intermediate loci lie on the imaginary axis, leading to starting and arrival points for the locus in a on this axis.

As an illustration, the closed-loop damping of the second mode on the pitch axis—due to the residual inertia I_r of the array—has been drawn as a function of this inertia (Fig. 11, continuous line). It appears that the closed-loop system becomes unstable for values of I_r under 20 m²kg (nominal value 24 m²kg). The closed-loop damping is also indicated, as well as the influence of a viscous torque on the motor equivalent to a natural relative damping of 0.01.

Several methods to improve the upper mode stability have been investigated. One of them is the phase control of the drive motor; using a varying phase ϕ of the motor control angle $\theta = \omega t + \phi$ as a control variable gives an additional phase lead to the control loop in the upper mode frequency bandwidth, thus increasing modal damping. It has been proved that, due to the sampling rate frequency, this result cannot be achieved through a classic lead-lag compensator.

Introduction of Torque Measurement

In this section the possibility of the measurement of the torque between the array and the vehicle is investigated.

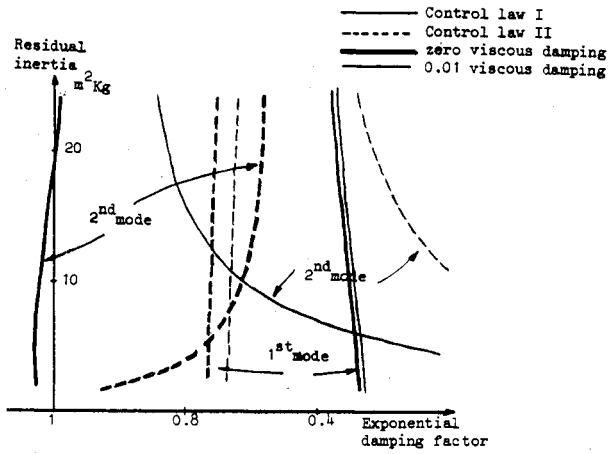

Fig. 11 Closed loop stability vs residual inertia.

Figure 8 may be turned into a two-input/two-output control diagram and two transfer matrices are introduced.

The first is transfer matrix S_1 relating the reaction wheel control torque u_x and array drive speed modulation ω_c to the vehicle attitude rate ω_r and torque between array and vehicle C_x (C_x is the output of block $G(s) = N(s)/D(s)$ in Fig. 8).

The second is transfer matrix S_2 relating the vehicle external disturbing torques C_u and the array drive disturbing torques Γ to ω_x and C_x

$$\begin{bmatrix} \omega_x \\ C_x \end{bmatrix} = \frac{1}{sD} \begin{bmatrix} \frac{D-N}{I_x} & -sN \\ -sN & -Ixs^2N \end{bmatrix} \begin{bmatrix} u_x \\ \omega_c \end{bmatrix} + \frac{1}{sD} \begin{bmatrix} \frac{D-N}{I_x} & -\frac{s^2N}{K_m} \\ -sN & -\frac{Ixs^3N}{K_m} \end{bmatrix} \begin{bmatrix} C_u \\ \Gamma \end{bmatrix} \tag{21}$$

It is worth noting that

$$S_2(s) = S_1(s) \begin{bmatrix} 1 & 0 \\ 0 & s/K_m \end{bmatrix} \tag{22}$$

Interest is now focused on noninteractive control design. The classical results on input-output noninteraction may not be applied due to the fact that the open-loop roots lie on the stability limit (or in its vicinity in the dissipative case). However it is possible to state and solve the noninteractive problem between disturbances and outputs for a given control law structure; i.e., design the control law in such a way that each disturbance affects one output and only one. Let us call the output vector Y, the control vector $\mathfrak{U}$, and the disturbance $\mathfrak{R}$. The transfer matrix representation of the system reads

$$Y = S_1 \mathfrak{U} + S_2 \mathfrak{R} \tag{23}$$

Let the control be elaborated from the output measurement by a transfer matrix

$$K(s) = \begin{bmatrix} k_{11}(s) & k_{12}(s) \\ k_{21}(s) & k_{22}(s) \end{bmatrix}$$

i.e., $\mathfrak{U} = KY$. Substitution in Eq. (23) and use of the relationship Eq. (22) leads to

$$Y = (I - S_1 K)^{-1} S_1 \begin{bmatrix} 1 & 0 \\ 0 & s/k_m \end{bmatrix} \tag{24}$$

The closed-loop transfer matrix will be diagonal if $S_1^{-1} - K$ is diagonal.

With

$$S_1^{-1} = \begin{bmatrix} -sI_x & 1 \\ 1 & \frac{D-N}{sNI_x} \end{bmatrix} \tag{25}$$

the condition reads

$$k_{12}(s) = k_{21}(s) = -1 \tag{26}$$

It leads to a disturbance of ω_x by C_u only, with control by transfer function $k_{11}(s)$; and to a disturbance of C_x by Γ only, with control by transfer function $k_{22}(s)$.

The consequences of these decoupling properties are very important because they allow one to design separately $k_{11}(s)$ to optimize the vehicle behavior vs the external disturbances

and $k_{22}(s)$ to optimize the array damping vs the motor disturbances. This is illustrated in the particular case of gain feedback

$$k_{11}(s)=a \qquad k_{22}(s)=d$$

the closed-loop transfer matrix reads

$$M(s)=\begin{bmatrix} \dfrac{D-N}{I_x}+dsN & -\dfrac{s^2N}{K_m}(b+1) \\ -N(c+1) & \dfrac{s^2N}{K_m}(a-I_x) \end{bmatrix} \tag{27}$$

$$sD+(b+c+bc-ad)sN+dIxs^2N-\frac{a}{I_x}(D-N)$$

and, with $b=c=-1$

$$\frac{\omega_x}{C_u}=\frac{1}{I_xs-a} \qquad \frac{C_x}{\Gamma}=-\frac{Ns^2I_x}{(D-N+dsI_xN)K_m} \tag{28}$$

The setting of a is, in any case, the control of a pure integrator, and for one mode only, $N=\Omega_f^2-\omega_f^2$, $D=s^2+\Omega_f^2$; and d allows arbitrary damping of the characteristic equation of the lower corner transfer function. A 0.7 damping has been chosen.

For several modes, the analysis of root locus associated to transfer function

$$H(s)=\frac{sIxN}{D-N} \tag{29}$$

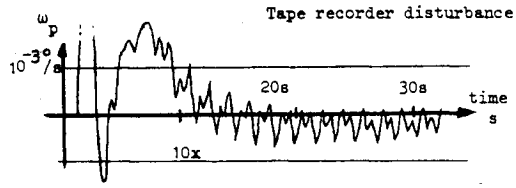

Fig. 12 Simulation of pitch attitude rate without damping and output filters.

describes the roots of the characteristic equation and illustrates the damping of the upper modes for the preceding setting of d.

These considerations are based on a continuous analysis, which is easier to handle than the discrete one, but Fig. 11 (dotted line) shows the important improvement of the closed-loop damping of the residual mode.

The interpretation of the decoupling condition is quite straightforward. The condition on ω_c ($\omega_c=-\omega_x$) is still, as indicated before, the setpoint of the rotor in the inertial frame, while the condition on C_x ($u_x=-C_x$) is a feed forward of the measured torque on the main control loop.

V. Simulations

Simulation Program Description

A detailed simulation model was built in the following manner.

1) The dynamic model was the fine model described in Sec. III with the four most significant modes of the array. Due to the order of magnitude of the time constants considered, the model was a stationary one around a given position on the orbit.

2) The sensor output filters and the noises were introduced.

3) Two basic control laws were compared; one without torque measurement (I), and the other with torque measurement and decoupling (II).

4) The three basic disturbances, start/stop of the recorder, rotation of the mirror, and harmonic disturbance of the array drive motor, were applied sequentially on a 70 s time interval.

Influence of the Couplings

The first aim of this global simulation was to check in the frame of the complete coupled model the analyses which were only tested axis by axis in the preceding sections. Figure 12 shows, for instance, the effect of a start/stop of the recorder for a conservative system at the node of the orbit without gyro output filters and with control law I. The coupling between the pitch and yaw is quite important, while the very weak damping of the closed-loop residual mode is apparent. The stability margin is so weak that the phase shift due to gyro filter is sufficient to lead to instability. A viscous damping on the motor had to be introduced to restore stability in the complete simulation case. A relative damping of 0.01 has proven satisfactory.

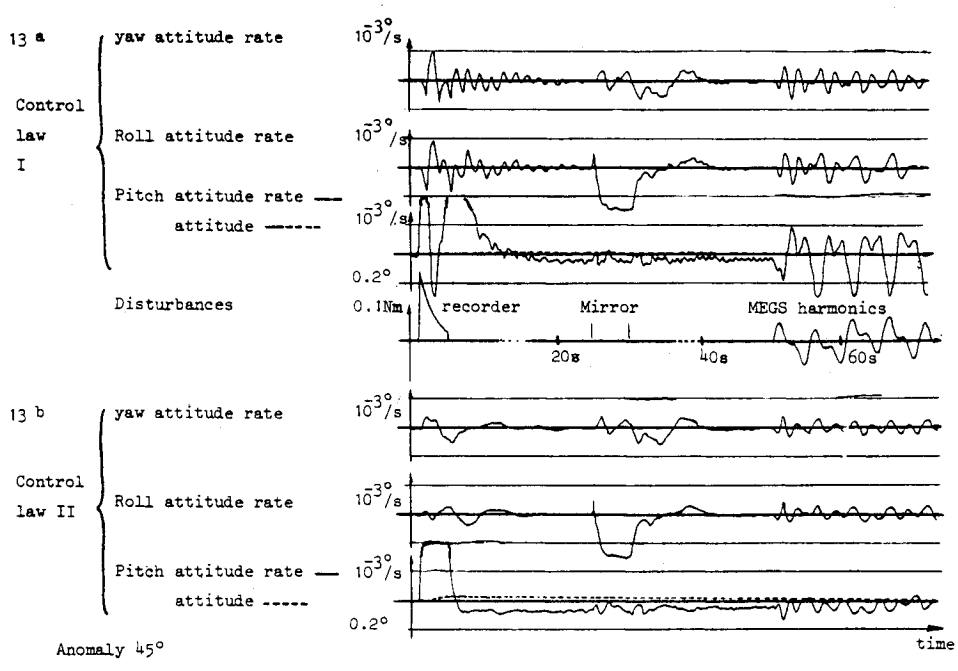

Fig. 13 Global simulations.

Figures 13a and 13b show the behavior of the controlled system with laws I and II for a 45 deg anomaly. The most striking feature, besides the much better performances achieved by control law II, is the quite important coupling between axes that leads to significant vibrations on the roll and yaw axes even during the harmonic disturbance on pitch axis.

Sensitivity Analysis

Extensive simulations where then made to evaluate the sensitivity of the control laws to mode frequency variations ($\pm 50\%$) and to residual inertia variations; modal data for a different angle between the wing of the array and the boom (for an orbit of a different local time) were also considered. The closed-loop performances remained quite acceptable in all cases, due to the robust properties of the control laws chosen.

VI. Conclusions

The fine pointing mode of the SPOT platform has been investigated in the following three areas.

The first was the derivation of a dynamic model of the spacecraft. The representation of the structural properties of the array by effective mass concept proved very efficient and two models were obtained; a first one keeping all the couplings between axes for reference simulation needs, and a second simplified one which allowed finding a sound control structure on the roll and yaw axes due to the dedication of each main flexible mode to each geometrical axis of the array.

The second was the design of control laws on roll and yaw axes which lead to stationary closed-loop performances as the spacecraft describes its orbit. The attitude rate is regulated in the array axes by a first-order digital network including integral control and closed-loop damping maximization, while a much slower outer loop keeps the attitude itself within the prescribed limits.

The third centered around the design of control laws on the pitch axis in the frame of a multi-input/multi-output control problem. The decoupling properties of the system allow damping the flexible modes in an active manner when a torque measurement is available. The performances without torquemeter are not as good and some passive damping must be assumed to achieve closed-loop stability. A trade off is necessary in the digital case between the attenuation of the harmonic disturbances and the destabilizing effect of the feedback from the gyro to the array drive motor. The choice of the control law structure is further based on a trade off between better performances and development cost of the torque measurement device.

Acknowledgment

This work was supported by C.N.E.S. under Contract 80-0607.[1]

References

[1] Chrétien, J.P., Reboulet, C., and Rodrigo, P., "Stabilisation de la Plate-forme multimissions en présence de modes flexibles," *Rapports techniques,* 7245/DERA No. 1, June 1980 and No. 2, Nov. 1980.

[2] *Manuel utilisateur de la plate-forme multimissions,* CNES/MATRA Espace M-MV-20425-MT, May 1981.

[3] Imbert, J.F. and Mamode, A., "The Effective Mass Concept in Base Motion Dynamics and Application to Solar Array Dynamics," *Nastran User's Conference,* Munich, F.R.G., 1977, pp. 343-354.